Pis'ma v ZhETF, vol. 96, iss. 8, pp. 546 – 551

Polarization tomography of bright states of light

I. N. Agafonov[+1)], *M. V. Chekhova*[+*], *T. Sh. Iskhakov*[*], *B. Kanseri*[*], *G. Leuchs*[*×]

[+] *Department of Physics, Lomonosov Moscow State University, 119991 Moscow, Russia*

[*] *Max Planck Institute for the Science of Light, 91058 Erlangen, Germany*

[×] *University of Erlangen-Nurnberg, 91058 Erlangen, Germany*

Submitted 17 September 2012

Polarization quantum tomography is performed on 4-mode squeezed vacuum states. Three-dimensional polarization quasiprobability functions are obtained and compared to that of an equal intensity coherent state. These distributions clearly demonstrate the difference in the polarization properties of the considered states. The reconstruction quality of the coherent state distribution is also analysed by comparing the theoretically and experimentally obtained shapes for this state.

Polarization properties of nonclassical light are important to quantum optics especially in the continuous-variables case where Stokes polarimetry method is often used [1]. Although it is an experimentally convenient method it only provides the basic polarization characteristics such as mean values and variances of the Stokes operators that are sufficient to characterize only Gaussian states. In the general case it is not feasible to analyze an infinite number of central moments, so in order to gain further insight into the state properties nonclassical polarization quasiprobability function (PQF) has to be considered. It was introduced by Karassiov and coworkers [2, 3] and has already been experimentally reconstructed for bright two-mode polarization squeezed (PS) vacuum [2, 4], bright PS coherent state and non-squeezed coherent state [5]. A state is called PS if the variance of at least one of its Stokes parameters is less than that of the coherent state of the same intensity.

In this paper we perform polarization quantum tomography to reconstruct the quasiprobability function $W(\mathbf{S})$ of bright four-mode PS vacuum states. Here, $\mathbf{S} = \{S_1, S_2, S_3\}$ are the corresponding Stokes observables. These are non-classical Gaussian states also known as macroscopic Bell states (MBS) that were theoretically predicted in [6] and experimentally observed in [7, 8]. Using coherent state reconstruction as an example, we analyze the reconstruction quality of our tomography technique.

PQF is defined as the Fourier transform of the polarization characteristic function $\chi(\mathbf{u})$ [2]

$$\chi(u_1,u_2,u_3) = \left\langle e^{iu_1\hat{S}_1+iu_2\hat{S}_2+iu_3\hat{S}_3}\right\rangle = \left\langle e^{i\mathbf{u}\cdot\hat{\mathbf{S}}}\right\rangle,$$

$$W(\mathbf{S}) = \frac{1}{(2\pi)^3}\int\int\int \chi(\mathbf{u})\, e^{-i\mathbf{u}\cdot\mathbf{S}} d\mathbf{u},$$

where the angle brackets denote averaging over the polarization state and $\hat{S}_{1,2,3}$ are the Stokes operators.

PQF serves as a tool to visualize a polarization state by depicting its polarization properties in a vivid manner. It also provides an easy way to calculate the distribution $p(S)$ for an arbitrary Stokes parameter S

$$S = \mathbf{S}\cdot\mathbf{n} = S_1\sin\theta\cos\varphi + S_2\sin\theta\sin\varphi + S_3\cos\theta, \tag{1}$$

where $\mathbf{n}$ is the unit normal vector and θ and φ are the spherical angles. The probability distribution $p(S)$ is given by the planar projection of PQF onto a line given by vector $\mathbf{n}$:

$$p(S) = \int\int\int \delta\left(\mathbf{S}'\cdot\mathbf{n} - S\right) W(\mathbf{S}')\, d\mathbf{S}'. \tag{2}$$

Inverting Eq. (2) and integrating by parts we get [3]

$$W(\mathbf{S}) = -\frac{1}{2\pi^2}\int_0^{\pi/2}\int_0^{2\pi}\left[\frac{\partial^2 p(\xi,\theta,\varphi)}{\partial\xi^2}\right]_{\xi=S}\sin\theta\, d\varphi\, d\theta. \tag{3}$$

This expression serves as the basis for polarization tomography and it turns out to be equivalent to an inverse Radon transform of the experimentally measurable histograms $p(S)$. Inversion symmetry of the Stokes operators measurement implies that it is sufficient to measure the histograms $p(S)$ within just a hemisphere in order to carry out a complete state reconstruction.

In this paper the PQF analysis is applied to MBS which are higher photon number generalizations of two-photon Bell states. The prepared MBS in our case contain four modes: two polarization and two wavelength

[1)] e-mail: ivan.agafonov@gmail.com

ones. Theoretically MBS have been considered in [6] and can be written as

$$|\Psi^{(\pm)}_{\rm mac}\rangle = \exp\left\{\Gamma\left(a_1^\dagger b_2^\dagger \pm b_1^\dagger a_2^\dagger\right) + \text{H.C.}\right\}|\text{vac}\rangle,$$
$$|\Phi^{(\pm)}_{\rm mac}\rangle = \exp\left\{\Gamma\left(a_1^\dagger a_2^\dagger \pm b_1^\dagger b_2^\dagger\right) + \text{H.C.}\right\}|\text{vac}\rangle, \quad (4)$$

where Γ is the parametric gain coefficient, $a^\dagger, b^\dagger$ are photon creation operators in the horizontal and vertical polarization modes, respectively and the subscripts 1, 2 denote wavelength modes. These states are generated by strongly pumping a standard setup used to produce two-photon Bell states. At the output of such a setup photon pairs, quartets, sextets and so on are produced in two wavelength and two polarization modes in such a way that the conjugate modes are correlated in photon numbers.

Similar to two-photon Bell states, all MBS are unpolarized in the first order of intensity. Thus their PQF are centered at the origin of the Stokes space. Theoretically each of the triplet states is completely squeezed in one of the three axes (Stokes observables) while antisqueezed in the other two axes resulting in a disk-like form of the PQF. The singlet state is completely squeezed in all three directions and thus unpolarized in all orders of intensity [9]. Experimental procedures introduce losses (detectors non-unity quantum efficiency, optical losses, imperfect signal and idler mode-matching) that result in non-perfect squeezing [10]. Fig. 1 shows the experimental expectation for isosurfaces of PQF of the triplet macroscopic Bell states with total losses of 30% taken into account. A coherent state PQF isosurface is also shown (yellow sphere). The singlet state PQF isosurface (not shown in Fig. 1) is contained within the coherent state PQF isosurface as it is squeezed in all directions. The triplet states isosurfaces smaller sizes are also less than those of the coherent state indicating squeezing along those directions, while bigger radii are greater than that of the coherent state indicating antisqueezing in those directions.

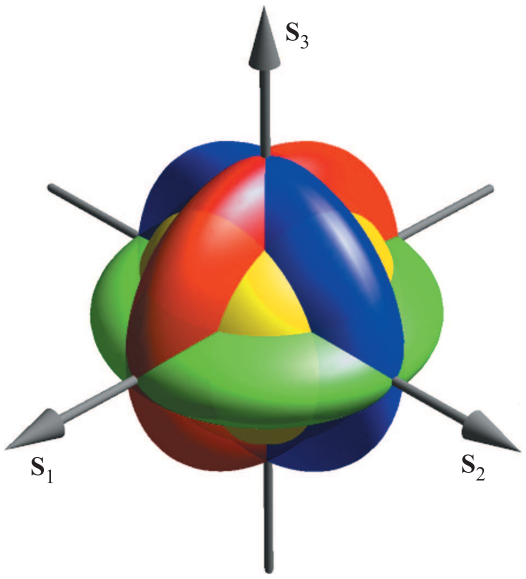

Fig. 1. (Color online) Experimental representation of PQF for triplet Macroscopic Bell states with losses in the setup taken into account: $|\Psi^+_{\rm mac}\rangle$ – blue, $|\Phi^+_{\rm mac}\rangle$ – green, and $|\Phi^-_{\rm mac}\rangle$ – red; coherent state (displaced to the origin) – yellow

The preparation part of the setup is depicted in Fig. 2. We generate the MBS $|\Phi^{(\pm)}_{\rm mac}\rangle$ via frequency-

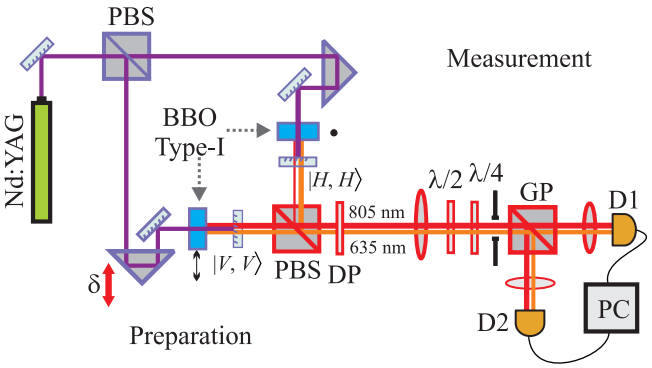

Fig. 2. – Orthogonally polarized squeezed vacuums are generated in two type-I BBO crystals and overlapped at a polarizing beamsplitter (PBS). The interferometer is balanced using trombone prisms. The dichroic plate (DP) is used for singlet state generation. The measurement part consists of a Glan prism (GP), a half-wave plate ($\lambda/2$), a quarter-wave plate ($\lambda/4$) and two detectors (D1 and D2) with their signals analyzed by the computer (PC)

nondegenerate parametric down-conversion (PDC) in two 2 mm beta barium borate (BBO) crystals with optic axes oriented in orthogonal (horizontal and vertical) planes. These crystals are placed into a phase-locked Mach–Zehnder interferometer (MZI) whose input and output beam splitters are polarizing ones. The crystals are pumped by a Nd:YAG laser third harmonic (wavelength $\lambda_p = 355$ nm, repetition rate 1 kHz, pulse duration 18 ps, and energy per pulse up to 0.2 mJ). At the input of the MZI the pump is 45° polarized in order to give equal contribution to PDC in both crystals. The pump radiation is cut off after the crystals using dichroic mirrors with 97% reflectivity and transmittance for the pump and the PDC radiation respectively and using a long pass (OG) filter (not shown in Fig. 2). Each crystal is a traveling-wave nondegenerate optical parametric amplifier with a two-color bright squeezed vacuum [10] at its output. Both squeezed-vacuum beams con-

taining wavelengths of $\lambda_1 = 635$ nm and $\lambda_2 = 805$ nm are orthogonally polarized and leave through the same port of the MZI. Depending on the phase δ between the squeezed-vacuum beams, the states $|\Phi^{(+)}_{\rm mac}\rangle$ or $|\Phi^{(-)}_{\rm mac}\rangle$ are generated at the output of the MZI. The phase δ can be varied by moving one of the mirrors, placed on a piezoelectric feed.

Preparation of the singlet state is the same as in Ref. [11]. The phase δ is fixed at π by measuring the variance of S_2: it is minimum in the case where the $|\Phi^{(-)}_{\rm mac}\rangle$ state is prepared. The $|\Phi^{(-)}_{\rm mac}\rangle$ state becomes $|\Psi^{(+)}_{\rm mac}\rangle$ in a 45°-rotated basis [12]. Using a dichroic wave plate placed into the output beam $|\Psi^{(+)}_{\rm mac}\rangle$ is transformed into $|\Psi^{(-)}_{\rm mac}\rangle$. The dichroic wave plate is made from a quartz crystal with its optical axis oriented at 45°. Its thickness of 170 μm is chosen in such a way that the ordinary-extraordinary phase delays introduced at the wavelengths λ_1 and λ_2 differ by π due to the dispersion. As a result, the plate introduces a π phase between the $a_1^\dagger b_2^\dagger$ and $b_1^\dagger a_2^\dagger$ terms in the expression for $|\Psi^{(+)}_{\rm mac}\rangle$ (see Eq. (4)).

The measurement part of the setup then filters the beam in the transverse wavevector by an iris aperture placed in the focal plane of a lens with 300 mm focal length. The crystals are also set 300 mm away from the lens. As shown in [10], the influence of the unmatched modes on the noise reduction is proportional to the number of photons per mode, so it is best to independently filter each wavelength of the beam in order to have the best possible mode matching. As it is experimentally complicated and the number of photons per mode in our case is relatively small (0.1), we use a single aperture.

The Stokes parameters measurement is realized by a Glan prism (GP) preceded by an achromatic half-wave plate (HWP, $\lambda/2$) and a zero-order quarter-wave plate (QWP, $\lambda/4$). The plates provide close phase-shifts at both wavelengths. The HWP and QWP oriented at α and β angles define a unit vector $\mathbf{n} = \{\cos\varphi\sin\theta, \sin\varphi\sin\theta, \cos\theta\}$ in Stokes space, where

$$\theta = \pi/2 - 2\beta, \qquad \varphi = 2\beta - 4\alpha. \tag{5}$$

This vector corresponds to an arbitrary Stokes observable $\hat{S}_n$ defined in a similar way to Eq. (1). The observable $\hat{S}_{\mathbf{n}}$ is measured as a difference of the photon numbers in the two output channels of the Glan prism. The beam is analyzed without separating the wavelengths or selecting single longitudinal or transverse modes, so $\hat{S}_{\mathbf{n}}$ is essentially multimode.

The photon numbers are measured pulse by pulse, using p–i–n diodes followed by charge-sensitive amplifiers [13]. The electronic noise is mostly caused by the amplification circuit and is equivalent to 180 input photons. On average each pulse contains about 10^5 photons, hence the shot noise (about 300 photons) exceeds the electronic noise almost twice. For each pump pulse, the output pulses of the detectors are time-integrated by means of an analog-digital card. The data are then processed to obtain the histograms of the measured Stokes parameters $p(S,\theta,\varphi)$ (see Eq. (3)).

According to Eq. (3), in order to calculate the PQF one has to know the Stokes observable distribution $p(S,\theta,\varphi)$ for all possible directions $\mathbf{n}$ (i.e., for all angles θ and φ). As it is not feasible in experiment, the integration and derivation in Eq. (3) has to be approximated by finite sums of discrete functions $p(S_i,\theta_j,\varphi_k)$ measured for a discrete set of angles θ_j and φ_k. In our case the states in consideration are Gaussian, so we approximate the obtained distributions by Gaussian functions

$$p_{jk}(S) \equiv \frac{A_{jk}}{\sqrt{2\pi}} \exp\left\{-\frac{(S-S_{0jk})^2}{2\sigma_{jk}^2}\right\}, \tag{6}$$

where A_{jk}, σ_{jk} and S_{0jk} are amplitudes, widths and displacements of the distributions obtained for θ_j and φ_k.

Substituting the distribution (6) into (3) we get

$$W(\mathbf{S}) = -\frac{1}{2\pi^2}\sum_{j=0}^{J}\sum_{k=0}^{K} p''_{jk}(S)\sin\theta_j\Delta\varphi\Delta\theta, \tag{7}$$

$$S = S_1\sin\theta_j\cos\varphi_k + S_2\sin\theta_j\sin\varphi_k + S_3\cos\theta_j,$$

where $p''_{jk}(S)$ is the second-order partial derivative with respect to S, $\theta_j = j\Delta\theta$, and $\varphi_k = k\Delta\varphi$, $J+1$ and $K+1$ are the numbers of measurements for each angle. The total number of measurements is thus $(J+1)\cdot(K+1)$.

In our experiment a total of 360 measurements are made for each state: the HWP is scanned from 0° to 87.5° with a step of 2.5° and the QWP is scanned from 0° to 45° with a step of 5°. According to Eq. (5), this results in set of measurements covering the upper hemisphere in the 3D Stokes space. Given that the noise and the signal are independent and that our states are Gaussian, the electronic noise is deducted from the measured signals by subtracting its variance from that of the measured signal.

By using an intensity stabilized He-Ne laser we prepare a coherent state (CS) that is used as a reference for quantifying squeezing. As our measurement system is adapted for the pulsed regime, a chopper rotating at a speed of 90 revolutions per second is used to obtain a coherent source with pulses of about 10 μs duration. The sum signal for the CS is set equal to that of the squeezed states. Our coherent state is not perfectly shot-noise limited due to some unavoidable excess fluctuations present

in the source so it is in fact a pseudo-coherent state (PCS).

Horizontal polarization of our PCS results in an unbalanced detection of all the Stokes observables S except for those that are in the $S_2 - S_3$ plane (the so called dark plane). This leads to a PQF elongated in the S_1 direction. In order to illustrate this effect we calculate the variance of the difference of photon numbers in two independent modes for a coherent state using the quantum model. In terms of the normalized second-order autocorrelation functions it is written as [14]:

$$\mathrm{Var}(N_-) = \left(g^{(2)} - 1\right) \langle N_- \rangle^2 + \langle N_1 \rangle + \langle N_2 \rangle , \qquad (8)$$

where $g^{(2)}$ is autocorrelation function (that coincides in this case with the crosscorrelation function as both modes have the same statistics), $N_- \equiv N_1 - N_2$ is the difference signal (in our case it is actually a Stokes observable). For an ideal coherent source $g^{(2)} = 1$ and the variance of difference photon number is simply given by the last two terms in Eq. (8), i.e. the shot noise level. In practice, for PCS, $g^{(2)} > 1$ and the first term can greatly affect the difference variance in the unbalanced case, especially when $N_- \gg 1$. To reconstruct the theoretical PQF we calculate the variance of the difference signal for each measurement using Eq. (8). The square root of this value is used as σ_{jk} in Eq. (7). To displace the state to the origin of the Stokes space we set S_{0jk} to zero in Eq. (7). The theoretical PQF reconstructed this way is almost indistinguishable from the experimental PQF with S_{0jk} reduced to zero. This proves that the unbalanced detection is the cause of non-spherical shape of PQF for our PCS. To quantify the similarity of the considered PCS PQFs we calculate the fidelity. Fidelity (Bhattacharyya coefficient) is a measure of similarity (overlap) of two PQFs and is defined as follows [15]

$$F_{ij} \equiv \sum_{\mathbf{S}} \sqrt{W_i(\mathbf{S}) W_j(\mathbf{S})}, \qquad (9)$$

where S spans the domain of PQFs with values greater than $1/e$ of their maximum values. F changes from 1 to 0, with 1 indicating that the PQFs are identical and 0 indicates that they don't overlap at all. The fidelity value calculated for the theoretical PQF and experimental PQF is 0.996.

Displacement of the PCS (which includes a strong classical component) PQF from the origin of the Stokes space is equal to the total number of photons n while its width corresponds to $\sqrt{n}$. In our case $n \approx 10^5$, so width and displacement of the PCS QPF differ by more than 300 times. This rises the problem of the reconstruction quality of the PQF for the PCS as it subtends a solid angle on the order of 10^{-5} in the Stokes space. To analyze this problem we calculate the theoretical fidelity of the PQF located at the origin using Eq. (8) and compare it with the PCS PQF displaced from its original position closer to the origin. The displacement is realized by reducing all the parameters S_{0jk} in Eq. (6). A plot showing fidelity versus the distance to the displaced PQF maximum is presented in Fig. 3. The

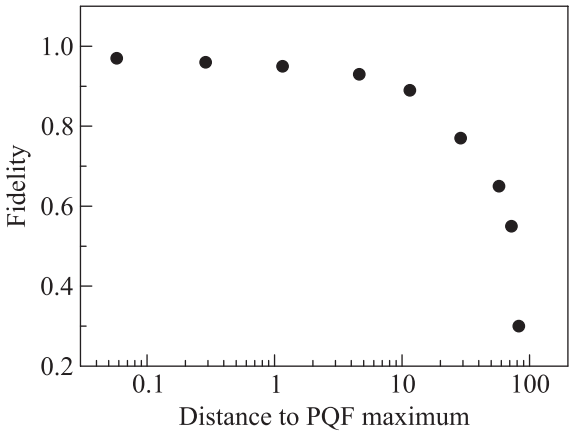

Fig. 3. Fidelity dependence on the distance to the PQF maximum value for the coherent state. The distance is normalized to the CS PQF width in the dark plane

distance is normalized to the CS PQF width in the dark plane. According to our results, the quality of CS PQF reconstruction from 360 measurements of the Stokes observables is satisfactory for displacements of up to 10 widths from the origin (the original position of the maximum is 580 widths away from the origin).

In order to reconstruct the original (non-displaced) PQF of a coherent or a squeezed coherent state more measurements are needed. It shall be noted that the reconstruction quality problem does not affect the MBS tomography as their PQF are located exactly at the origin of the Stokes space (see Fig. 1).

The results of the experimental data processing using Eq. (7) are shown in Fig. 4. The $3D$ images ((a), (e), and (i)) were obtained by plotting the isosurface $W(\mathbf{S}) = \max W(\mathbf{S})/\sqrt{e}$ of the PQFs. The images below the 3D plots are 2D contour plots (colour coding scales are different) of the corresponding states: $W(S_1, S_2, 0)$ for (b), (f), and (j); $W(0, S_2, S_3)$ for (c), (g), and (k); $W(S_1, 0, S_3)$ for (d), (h), and (l). Since the pseudo-coherent state is horizontally polarized, its PQF is greatly displaced from the origin in contrast with unpolarized singlet and triplet states. PCS polarization quasiprobability function has its maximum at point ($346{\cdot}10^3$, $31.5{\cdot}10^3$, $14{\cdot}10^3$) photons in the Stokes space. Nonzero values of S_1 and S_2 indicate that the

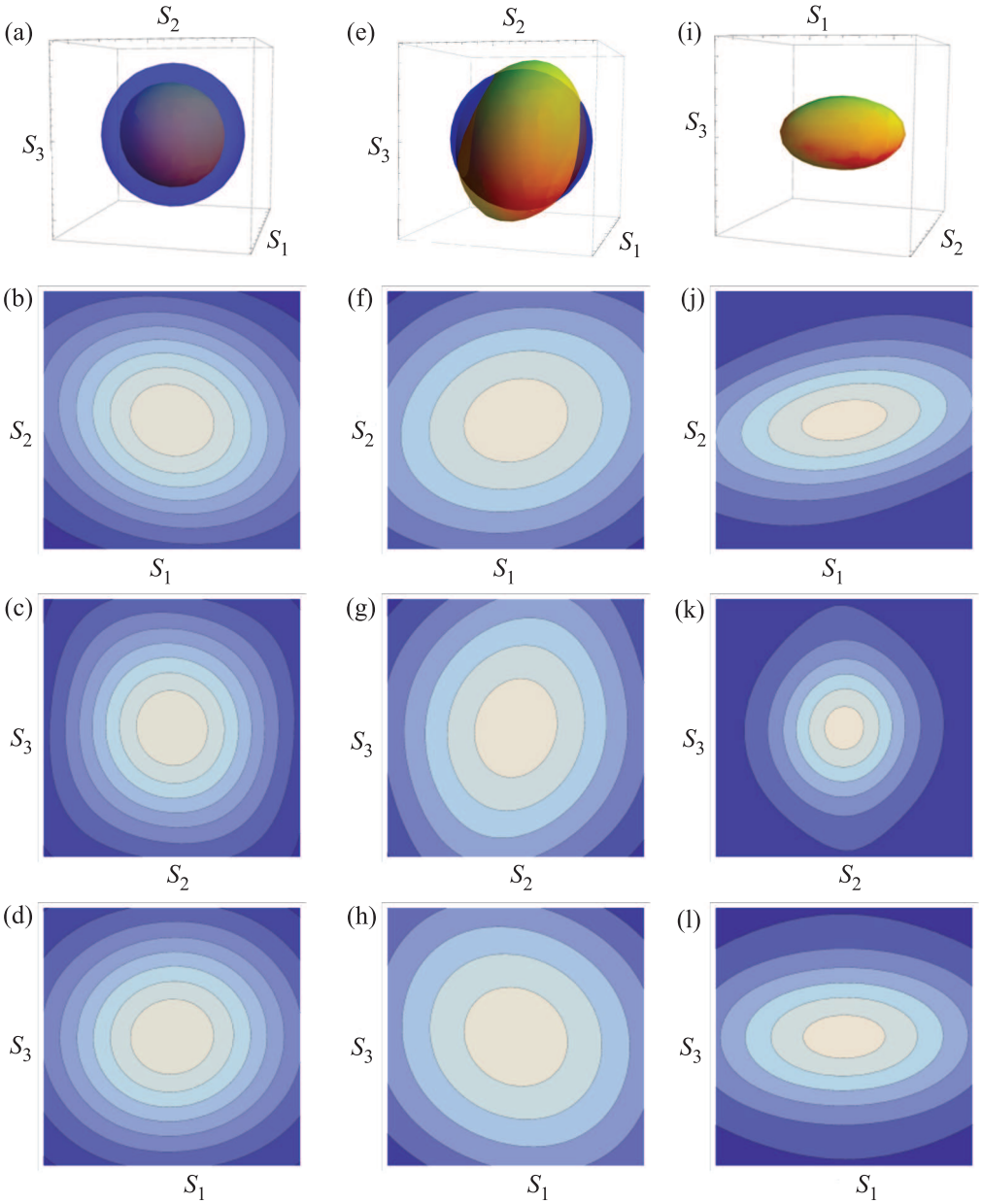

Fig. 4. (Color online) Polarization quasiprobability functions $1/\sqrt{e}$ isosurface in $3D$ and its $2D$ contour plots (colour coding scales are not fixed) for: (a)–(d) singlet, (e)–(h) triplet and (i)–(l) pseudo-coherent states. Contour plots (b), (f), (j) correspond to $S_1 - S_2$ plane, (c), (g), (k) – to $S_2 - S_3$ plane, (d), (h), (l) – to $S_1 - S_3$ plane. Semi-transparent blue spheres on (a) and (e) represent the corrected coherent state

PCS is not perfectly (100%) horizontally polarized owing to the fact that the light beam passes through several reflections by the mirrors present in the setup. Taking into account the above mentioned reconstruction quality problem, the parameters S_{0jk} in Eq. (6) were reduced to 0 when plotting the PQF function in Fig. 4i–l. In order to visualize the difference between the MBS state and the CS, a blue semi-transparent sphere is plotted on Fig. 4a and e. It represents the PQF of a corrected CS with the radius equal to that of the PCS PQF in the dark plane.

To characterize squeezing, the variance of each Stokes observable S of the observed state $\Delta^2 S(\Psi)$ has to be compared to that of a shot-noise-limited state, i.e. a coherent state $\Delta^2 S(\mathrm{coh})$. The width of the PQF (shown in Fig. 4) along direction $\mathbf{n}$ corresponds to the Stokes observable standard deviation ΔS, so one can easily estimate the amount of squeezing using the PQF according

to the following definition of Polarization Noise Reduction Factor (PNRF)

$$\mathrm{PNRF}(\mathbf{n}) \equiv \frac{\Delta^2 S(\Psi)}{\Delta^2 S(\mathrm{coh})}. \qquad (10)$$

Depending on the choice of the Stokes observable S, the amount of squeezing for a given state will, in the general case, vary. In order to calculate and compare the PNRF along $S_1 - S_3$ directions for the singlet and triplet states we approximate the reconstructed PQFs by a $3D$ Gaussian functions of the form

$$\widetilde{W}(\mathbf{S}) = \frac{A}{\sqrt{2\pi}} \exp\left\{-\frac{S_1^2}{2\sigma_1^2} - \frac{S_2^2}{2\sigma_2^2} - \frac{S_3^2}{2\sigma_2^3}\right\}, \qquad (11)$$

where A is the amplitude and $\sigma_{1,2,3}$ are the widths. In order to account for the non-spherical shape of our pseudo-coherent state PQF we approximate it by a Gaussian function (11) assuming $\sigma_2 = \sigma_3 = \sigma_{\mathrm{coh}}$. In this case the true width of the CS PQF is given by the σ_{coh} as it corresponds to the dark plane (balanced detection). This width is used to calculate the $\Delta^2 S(\mathrm{coh})$ in Eq. (10) and to plot the semi-transparent blue spheres corresponding to the corrected CS PQF in Fig. 4. Substituting the obtained widths for the singlet and triplet states into (10) we get the PNRF values along the $S_1 - S_3$ directions (see Table).

PNRF for singlet and triplet state along $S_1 - S_3$ directions

State	PNRF(S_1)	PNRF(S_2)	PNRF(S_3)
$\lvert\Psi_{\mathrm{mac}}^{(-)}\rangle$	0.74	0.50	0.58
$\lvert\Phi_{\mathrm{mac}}^{(-)}\rangle$	1.31	0.77	1.17

As one can see from Fig. 4, the singlet state PQF is very similar to the theoretical one: it is located at the origin of the Stokes space showing that all the Stokes parameters are zero (the state is unpolarized in the first order of intensity) and it is smaller than the CS PQF in all directions. Having almost spherical isosurface its mean PNRF value is 0.6 (see Table). The triplet state PQF clearly shows its oblong shape: it is squeezed in S_2 direction (smaller than the CS) and antisqueezed in S_1 and S_3 directions (bigger than the CS). This indicates that the prepared triplet state is $|\Phi_{\mathrm{mac}}^{(-)}\rangle$ (see Fig. 1).

In conclusion we have experimentally reconstructed polarization quasiprobability functions for two bright four-mode squeezed vacuum states (singlet and triplet) and for a pseudo-coherent state. The singlet state $|\Psi_{\mathrm{mac}}^{(-)}\rangle$ PQF has an almost spherical isosurface and the triplet state $|\Phi_{\mathrm{mac}}^{(-)}\rangle$ demonstrates its oblate shape. We have demonstrated that the quality of PQF reconstruction for a pseudo-coherent state (measured as fidelity) degrades as the PQF maximum gets further away from the origin. It is clear that much more than 360 measurements are required to reconstruct highly displaced states with good fidelity values. At the same time, this is not an issue for reconstructing unpolarized states (like MBS) PQFs as they are located at the origin of the Stokes space.

We acknowledge the financial support of the Russian Foundation for Basic Research, grants #10-02-00202, 11-02-01074, and 12-02-00965. I. N. A. acknowledges support from the Dynasty Foundation. T.Sh.I. acknowledges funding from Alexander von Humboldt Foundation.

1. W. P. Bowen, R. Schnabel, H.-A. Bachor et al., Phys. Rev. Lett. **88**, 093601 (2002).
2. V. P. Karasev and A. V. Masalov, Opt. Spec. **91**, 558 (2001).
3. V. P. Karassiov, J. Russ. Laser Res. **26**, 484 (2005).
4. V. P. Karasev and A. V. Masalov, JETP **99**, 51 (2004).
5. Ch. Marquardt, J. Heersink, R. Dong et al., Phys. Rev. Lett. **99**, 220401 (2007).
6. V. P. Karassiov, J. Phys. A **26**, 4345 (1993).
7. T. Sh. Iskhakov, M. V. Chekhova, G. O. Rytikov et al., Phys. Rev. Lett. **106**, 113602 (2011).
8. B. Kanseri, T. Iskhakov, I. Agafonov et al., Phys. Rev. A **85**, 022126 (2012).
9. T. Sh. Iskhakov, I. N. Agafononv, and M. V. Chekhova, Phys. Rev. A **84**, 045804 (2011).
10. I. N. Agafonov, M. V. Chekhova, and G. Leuchs, Phys. Rev. A **82**, 011801(R) (2010).
11. A. V. Burlakov, S. P. Kulik, and G. O. Rytikov, JETP **122**, 738 (2002).
12. G. Leuchs, R. Dong, and D. Sych, New J. Phys. **11**, 113040 (2009).
13. T. Sh. Iskhakov, M. V. Chekhova, and G. Leuchs, Phys. Rev. L **102**, 183602 (2009).
14. T. Iskhakov, A. Allevi, and D. Kalashnikov, Eur. Phys. J. Special Topics **199**, 127 (2011).
15. A. Bhattacharyya, Bull. Calcutta Math. Soc. **35**, 99 (1943).